Electron-Induced Chemistry of Methanol on Ag(111)

A. L. Schwaner and J. M. White*

Center for Materials Chemistry, Department of Chemistry and Biochemistry, University of Texas, Austin, Texas 78712

Received: July 2, 1997; In Final Form: October 5, 1997[⊗]

On Ag(111) at 120 K, there is no thermal dissociation of methanol, but electron irradiation induces fragmentation. After irradiation of monolayers, temperature-programmed desorption (TPD) contains water (at 172 K), methane (190 K), hydrogen (200 K), and formaldehyde (225 and 255 K). X-ray photoelectron spectroscopy (XPS) intensities before and after irradiation are comparable, indicating little product ejection during irradiation. For multilayers there is an additional product in TPD—glycolaldehyde or methyl formate. During irradiation, the work function rises, reflecting adsorbate structural changes. The XPS, TPD, and work function measurements return to the clean surface values upon heating from 120 to 450 K. Evidently, impact ionization initiates the chemistry, and the resulting cations fragment, reneutralize, and chemisorb to Ag. Dissociation of a C−H bond to form $H_2C_{(a)}O_{(a)}H$ or a C−O bond to form $C_{(a)}H_3$ and $O_{(a)}H$ accounts for the products found after relatively short irradiations. Evidence for $O_{(a)}H$ bond breaking by electron irradiation appears only after long irradiation times. Formaldehyde oligomers, stabilized by interactions with Ag, are proposed to account for the H_2CO desorption at 255 K.

1. Introduction

Methanol chemistry is of significance to industry, exemplified by its partial oxidation to formaldehyde over silver- or copper-based catalysts.[1] These considerations have motivated numerous surface science investigations of methanol,[2] some emphasizing intermediates generated upon adsorption and during subsequent thermal processing. Wachs and Madix[3] showed that formaldehyde formation on an oxygen-precovered Cu(110) surface proceeds via a methoxy, $CH_3O_{(a)}$,[4] surface intermediate. This pioneering work has been followed by extensive investigations that employed surface science tools (e.g., X-ray photoelectron spectroscopy (XPS), high-resolution electron energy loss spectroscopy (HREELS), infrared spectroscopy (IR), and ultraviolet photoelectron spectroscopy (UPS)) to characterize oxygenates on a variety of single-crystal, polycrystalline metal and metal oxide surfaces. The work reported here is one of a series of studies that focus on nonthermal activation of adsorbates.[5−7]

Methanol−metal substrate systems can be divided into three groups based on the substrate: (1) active transition-metal surfaces, e.g., Ni, Pt, Pd, Fe, and Ru, (2) aluminum and its alloys, and (3) less active coinage metals, e.g., Cu and Ag. A significant fraction of monolayer coverage dissociates thermally on the active metals. CO and H_2 often dominate the products in temperature-programmed desorption (TPD). Methoxy intermediates have been identified, by XPS, HREELS, UPS, or IR, on Ni(110),[8,9] Ni(111),[10,11] Ni(100),[12−15] poly-Ni,[16] Pd(100),[15,17] Pd(111),[18,19] Fe(100),[20−23] Fe(110),[24] Mo(100),[25] Ru(001),[26,27] Rh(111),[28] Pt(110),[29] Pt(100),[30] Pt(111),[31] poly-Pt,[32] and W(100).[33] Formaldehyde was synthesized thermally when methanol was adsorbed on preoxidized Pd(111),[18] Fe(100),[21] and Ru(001),[26] and water was detected from decomposition of methanol on preoxidized Pt(110)[29] and Pt(100).[30] Preadsorbed sulfur on Fe(100)[22] suppressed methoxy formation and, hence, methanol decomposition.

On Al(111),[34] FeAl(110),[35] and polycrystalline Al,[36] methanol decomposes via a methoxy intermediate, but the products are $CH_{4(g)}$, $H_{2(g)}$, $C_{(a)}$, and $O_{(a)}$. Energetic electron and ion beams induce decomposition of methoxy species adsorbed on Al(111),[37] resulting in C−O (dominant) and C−H bond scission and leading to CH_x, C, and O surface species.

On the coinage metals, such as Cu(100),[38] Cu(110),[3,39,40] Cu(111),[41] Ag(110),[42−44] Ag(111),[15,45] and poly-Ag,[46] negligible thermal chemistry accompanies low-temperature adsorption (ca. 100 K). Substrate reactivity is enhanced if precovered with atomic oxygen—water, hydrogen, formaldehyde, and methyl formate have been found in subsequent TPD. Formaldehyde can be further oxidized to carbon dioxide and water in the presence of excess surface oxygen.[43] Preadsorbed oxygen acts as a Bronsted base, deprotonating the hydroxyl hydrogen and resulting in adsorbed methoxy and hydroxyl. There is evidence that hemiacetyl alcoholate, $H_2C(OH)OCH_3$, forms on O-precovered Ag(111) from the interaction of adsorbed methoxy and formate intermediates.[45]

That Ag(111) thermally activates few adsorbates makes it an attractive candidate for examining nonthermal (electron or photon) activation.[5,6] In this paper, we characterize the electron-induced decomposition of CD_3OD and CH_3OD, particularly monolayers, as part of our ongoing study of the electron-induced chemistry of oxygenates.[7,47,48] Based on XPS and TPD, electrons with energies exceeding the ionization potential initiate fragmentation with very little ejection of carbon- or oxygen-containing species. Based on isotope distributions in the TPD products, C−O and C−H bond breaking dominate, while O−H cleavage makes a minor contribution. In XPS and TPD we see evidence that heating after irradiation leads to thermal reactions that result in new adsorbed species and to desorption of H_2O, CH_4, H_2, and H_2CO.

2. Experimental Section

The experiments were performed in a standard stainless steel ultrahigh-vacuum (UHV) chamber[7] equipped for TPD, Auger electron spectroscopy (AES), XPS, and UPS. Work function changes ($\Delta\phi$) were calculated from shifts of the secondary emission onsets in UPS spectra.

The Ag(111) crystal was prepared and cleaned by standard methods; cleanliness was confirmed by AES. Methanol, CD_3-

[⊗] Abstract published in *Advance ACS Abstracts,* November 15, 1997.

S1089-5647(97)02136-6 CCC: $14.00

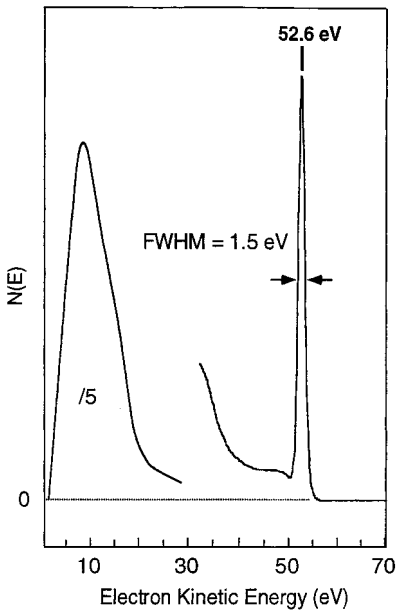

Figure 1. Electron energy distribution from electron source set at nominally 52 eV.

OD or CH_3OD, was used as received, and mass spectrometry verified the purity, including isotopic purity (99%). To minimize background CH_4 problems (see below), CH_3OH was not used. Dosing was accomplished through a leak valve connected to a directed capillary array, with the delivery tube terminating 0.5 cm away from the Ag(111) surface. With the sample turned away from the doser, the ion gauge reading was increased, $\Delta p = 5 \times 10^{-10}$ Torr, by opening the leak valve. The sample (120 K) was then quickly rotated in front of the doser for a time predetermined to give the desired coverage. About 55 s was required to adsorb a monolayer.

The open source of the mass spectrometer was used for electron irradiation. Figure 1 shows a typical electron energy distribution measured with the cylindrical mirror analyzer located across the chamber. The primary peak is located near 50 eV with a fwhm of 1.5 eV. The intensity in the 0−20 eV region is attributable to secondary electrons generated by interactions in the ionizer, in the detector, and on a portion of the sample mount which, although moved away from its normal position, still intercepts a portion of the electron flux from the mass spectrometer filament.

To initiate irradiation, the dosed sample was rotated into line-of-sight with the mass spectrometer for a predetermined time. We could not bias the sample and simultaneously control the temperature ramp, so the sample was rotated 90° away from line-of-sight to terminate electron dosing. In this position, TPD spectra were taken with a heating rate of 1.5 K/s between ~110 and 690 K. Clean Ag(111) was irradiated and the resulting TPD subtracted as background from each of the reported spectra. Adjustments for fragmentation patterns that overlap were also made.

To test whether species were ejected during irradiation, isothermal mass spectra (ISOMS) were taken while dosing with electrons. A negatively biased sample was positioned in line-of-sight with the mass spectrometer for, typically, 30 s while monitoring several signals. Then, while continuing to monitor the mass spectra, we removed the bias, allowing the electron flux ($\sim 10^{+14}$ e^- cm^{-2} s^{-1}) to irradiate the adsorbate−substrate interface.

Fragmentation patterns for CD_3OD and CH_3OD were employed in evaluating the TPD spectra. Two points are noteworthy for CD_3OD: (1) gas-phase impact ionization followed by fragmentation leads to D_2COD^+, not D_3CO^+; and (2) the D_2CO^+ signal (32 amu) is negligible.[49] These are important factors in describing methanol's electron-induced surface chemistry. With the exception of CD_3^+, which was higher due to mass analyzer tuning, the fragmentation patterns were consistent with literature values.[49]

For XPS, we operated the cylindrical mirror analyzer with a 50 or 100 eV pass energy, depending on the signal intensity. The raw data were subjected to standard three-point smoothing and were then fit to Gaussian−Lorentzian (G−L) functions (85% G−15% L) with fixed full widths at half-maximum (fwhm). The latter were established in calibration data taken for known samples: 2.2 ± 0.1 for C(1s) and 2.1 ± 0.1 eV for O(1s) at 50 eV pass energy and 3.1 ± 0.1 and 3.0 ± 0.1 eV for 100 eV pass energy. Using these fixed widths and a Shirley background subtraction, the MgKα excited XPS core level spectra for C(1s) and O(1s) were fit to the minimum number of peaks required to match the overall width and shape of the experimental spectra. Particularly when the features overlap strongly, this method does not preclude contributions from additional species.

Absolute coverages, in molecules cm^{-2}, were calculated from the C(1s) and/or O(1s) XPS peak areas using a standard and the relative elemental sensitivities established for our instrument. The standard is 4.6×10^{14} cm^{-2} of atomic iodine in a readily established $(\sqrt{3} \times \sqrt{3})R30°$ structure formed on Ag(111).[50] In our experiments, this structure was formed by the thermal dissociation of CF_3I, and the relative elemental sensitivities were taken from a literature tabulation.[51]

UPS spectra were collected using a conventional helium discharge lamp with the sample biased negatively, so the secondary onset was easy to identify. Work function changes, $\Delta\Phi$, were determined from shifts in this onset.

3. Results

In the following sections, evidence is presented for (1) reversible nondissociative adsorption and desorption, (2) increased sticking coefficient in multilayers, (3) electron-induced decomposition of CD_3OD and CH_3OD; (4) negligible ejection of species containing C or O during electron exposure (except for multilayers), and (5) desorption of hydrogen, water, methane, and formaldehyde in postirradiation TPD.

Thermal Chemistry of CD_3OD. *TPD without Electrons.* To initiate our study, we searched for but found no evidence for thermal dissociation of CD_3OD during adsorption at 120 K and subsequent TPD. The 36, 34, 30, and 18 amu ion signals matched the gas-phase fragmentation pattern and tracked each other as a function of temperature. XPS and $\Delta\Phi$ indicate a clean Ag(111) surface after TPD, confirming reversible adsorption and desorption.

The CD_3OD^+ TPD spectra (Figure 2) show that at low coverage, curve (a), there is one desorption peak at ~160 K. As the coverage increases, this peak shifts to slightly lower desorption temperature, 157 K, and saturates, curve d. Further adsorption leads to an unsaturable TPD peak, initially at 142 K but slowly shifting to higher temperatures with increasing coverage (146 K for curve g); this is typical of molecular multilayers. Given the saturation behavior of the 157 K peak and the opposite behavior of the 142 K peak, we assign curve d to monolayer coverage. The monolayer desorption temperature agrees with values found for other Ag substrates,[52] and the multilayer desorption temperature, which should be independent of substrate, is in agreement with literature values for several substrates.[52]

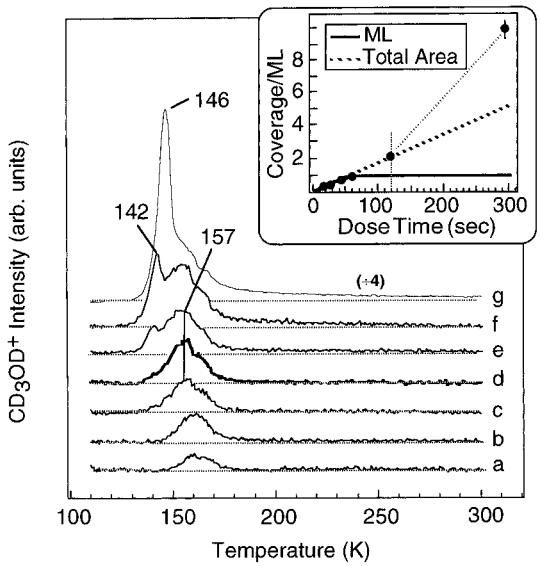

Figure 2. TPD plot of CD_3OD as a function of increasing dosing time at 120 K: (a) 20, (b) 30, (c) 45, (d) 55, (e) 60, (f) 120, and (g) 300 s at $\Delta p = 5 \times 10^{-10}$ Torr. The bold curve (d) is defined as one monolayer of CD_3OD. (inset) Plot of the integrated peak area with increasing CD_3OD exposure.

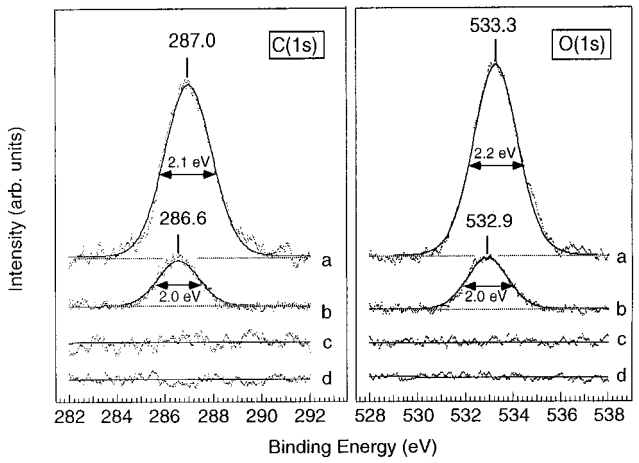

Figure 3. C(1s) and O(1s) XPS for (a) multilayer and (b) monolayer CD_3OD, (c) after flashing to 450 K, and (d) clean Ag(111) substrate.

The inset in Figure 2 shows the monolayer (157 K) and the total TPD peak areas as a function of dose time. The coverage grows linearly up to 120 s, but the slope definitely increases between 120 and 300 s. Apparently, collisions of warm CD_3OD with cold Ag(111) are less effective in exchanging energy than are collisions between warm CD_3OD and cold adsorbed CD_3OD. Detailed TPD analysis reveals a small shoulder (<10% at 1 ML) near 165 K for all coverages. This is attributed to defect sites, since it becomes more intense when CD_3OD is adsorbed onto a sputtered, but not annealed, surface.

XPS without Electrons. Core level XPS for the multilayer (a), the monolayer (b), and surfaces heated to 450 K (c) are compared to clean Ag(111) (d) in Figure 3 (50 eV pass energy). As expected for molecular adsorption, the C(1s) and O(1s) spectra are simple; each has one peak, characteristic of a single chemical environment. The smoothed data (dots) were fit as described in section 2. The results (solid curves) give the peak positions and widths (fwhm) listed in Table 1. On the basis of the calibration described earlier, we calculate an absolute coverage of $8 \times 10^{+14}$ cm^{-2} for monolayer CD_3OD. The binding energy (BE) values for multilayer and monolayer CD_3OD are well within the range reported for methanol adsorption on other surfaces.[3,20,29,36,39,43,52,53] The 0.4 eV BE increase for the multilayer is attributed to a common final state effect in which core hole screening weakens as the coverage of CD_3OD increases.

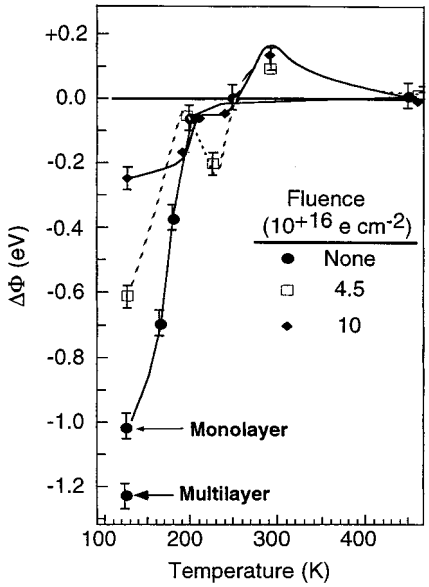

Figure 4. Variation of $\Delta\Phi$ with temperature after dosing 3 ML of CH_3OD on Ag(111) at 120 K (filled circles) and after irradiating 1 ML of CH_3OD with 4.5×10^{16} e^- cm^{-2} (open squares) and 1×10^{17} e^- cm^{-2} (filled diamonds). Curves drawn to guide the eye.

SCHEME 1: Geometry of Adsorbed Methanol

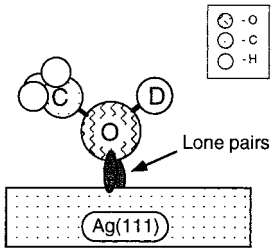

TABLE 1: XPS Peak Positions (BE) and Widths for CD_3OD on Ag(111)

coverage, ML	core level	binding energy, eV	fwhm, eV
1	C(1s)	286.6	2.0
6	C(1s)	287.0	2.1
1	O(1s)	532.9	2.0
6	O(1s)	533.3	2.2

Flashing the substrate to 450 K, curves c, gives traces indistinguishable from those measured before dosing CD_3OD, curves d. Coupled with TPD, this confirms the lack of thermal decomposition of CD_3OD.

Work Function Changes without Electrons. Work function changes as a function of CH_3OD coverage and annealing temperature, without electron irradiation, are displayed in Figure 4 (circles). The work function change was −1.2 eV for multilayer coverage and −1.0 eV for monolayer CH_3OD. When a monolayer was heated, the work function increased sharply between 120 and 180 K, and as expected, the clean surface value was reached between 200 and 240 K. The work function decrease when CD_3OD is adsorbed suggests that the surface dipole has its "+" end toward the vacuum in the vacuum−adsorbate interface. This is consistent with models that orient, albeit very weakly, the oxygen lone pairs as depicted in Scheme 1. Below, we discuss the effects of the electron fluences displayed in Figure 4.

Electron-Induced Chemistry of CD_3OD and CH_3OD. *Reaction Path for Electron-Induced Chemistry.* Before offering

SCHEME 2: Reaction Scheme—Monolayer

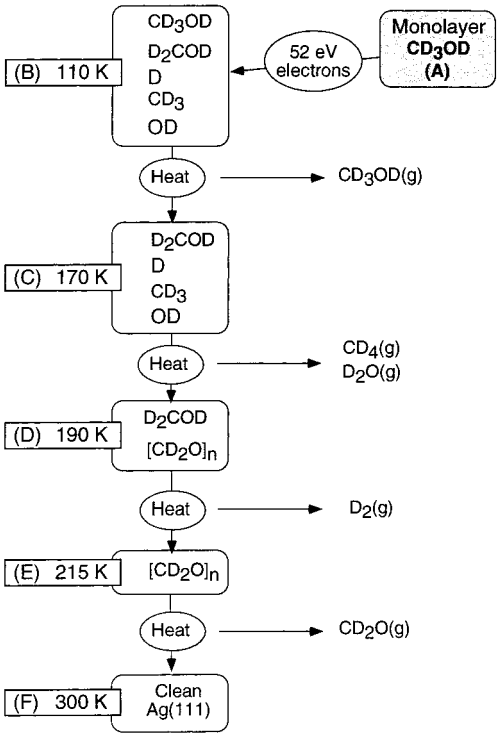

details, we present a brief overview. Using CD_3OD as an example, Scheme 2 diagrams the proposed major electron-induced (top) and subsequent thermally activated reactions (top to bottom) that occur when the initial coverage is 1 ML and the electron fluence is $\leq 4.5 \times 10^{15}$ e$^-$ cm^{-2}. With the substrate held at 120 K, 52 eV electrons incident on monolayer CD_3OD (A) dissociate predominately C−D bonds to form $D_2C_{(a)}O_{(a)}D$ and $D_{(a)}$ and, to a lesser extent, C−O bonds to form $C_{(a)}D_3$ and $O_{(a)}D$ (B). Upon heating after irradiation, residual $CD_3O_{(a)}D$ desorbs below 170 K with no thermal surface reactions (C). As the temperature is increased to 190 K, $D_{(a)}$ is activated and hydrogenates $C_{(a)}D_3$ and $O_{(a)}D$ to form and desorb CD_4 and D_2O. Thermally activated O−D bond breaking also occurs, forming adsorbed oligomers, $[D_2CO]_n$, (D), and producing more than sufficient $D_{(a)}$ to remove all of the methyl and hydroxyl groups. At slightly higher temperatures, D_2COD decomposes to release D_2CO and form additional $D_{(a)}$ which recombines to desorb D_2. Additional formaldehyde oligomers, $[D_2CO]_n$, are also formed (E). The oligomers decompose to release formaldehyde, leaving a clean Ag(111) substrate at 300 K (F).

We now turn to detailed evidence for these proposed steps.

Electron-Induced Chemistry. The 36 amu parent ion (CD_3OD^+) TPD traces decay with electron irradiation time (fluence varies linearly with time), and the peak area changes with fluence (Figure 5, upper and lower panels). The shape of the 157 K curve is independent of the dose time, and the areas decay in approximately first-order fashion with a cross section of $(7.8 \pm 0.4) \times 10^{-18}$ cm^2, reflecting an efficiency (loss per incident electron) between 0.1 and 0.01. The decay slows (smaller cross section) for large fluences where ~0.4 of the initial coverage remains. This trend is attributed to accumulation of dissociation products that occupy chemisorption sites and retard further electron-induced dissociation of CD_3OD.

Figure 6 plots the cross section as a function of the incident primary electron energy, holding the fluence constant at $4.5 \times 10^{+16}$ e$^-$ cm^{-2}. The decay is measurable at 14 eV but not at 9 eV. The experimentally reachable lower energy limit is ~8 eV. The extrapolated threshold is 12.5 eV. The gas-phase

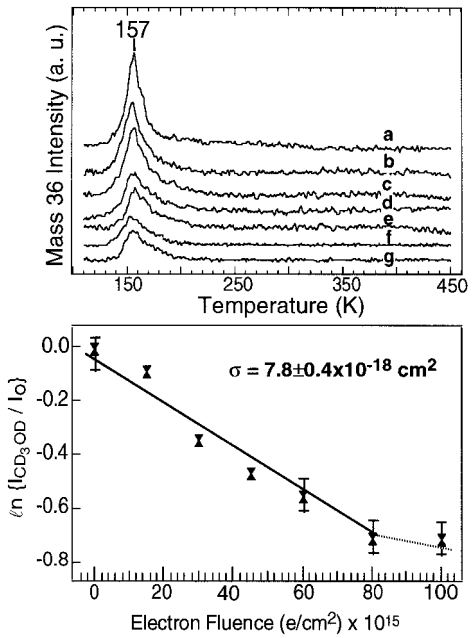

Figure 5. (top) Parent TPD spectra taken after 50 eV electron irradiation of 1 ML of CD_3OD at 120 K with the following fluences: (a) 0, (b) 1.5, (c) 3.0, (d) 4.5, (e) 6.0, (f) 8.0, and (g) 10×10^{16} e$^-$/cm^2. (bottom) Semilogarithmic plot of the fractional decrease in CD_3OD TPD peak area. Error bars determined from duplicate experiments. The solid line in the bottom figure is a linear fit, and the dotted extension is meant to indicate that the slope decreases for large fluences.

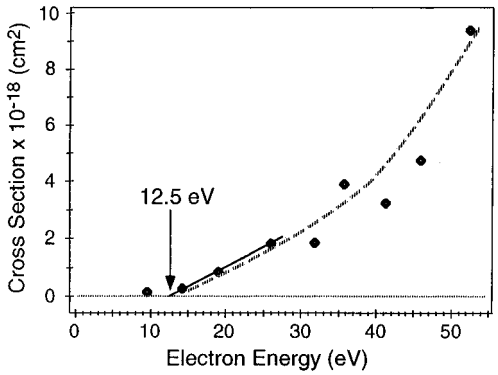

Figure 6. Cross section for loss of 1 ML CD_3OD as a function of incident electron energy. Dashed line is a guide for the eye.

ionization potential is 10.8 eV.[54] Keeping in mind that the incident electrons generate a continuous distribution of lower energy secondaries (Figure 1), we conclude from Figure 6 that impact ionization dominates the initial excitation. Other lower energy electron excitation modes, e.g., electron attachment and impact excitation, may contribute, but the cross sections must lie below 10^{-19} cm^2.

Ejection during Irradiation. Using ISOMS, described in section 2, we searched for species ejected during 52 eV irradiation (0.1×10^{14} e$^-$ cm^{-2} s^{-1}) for 600 s of monolayer CD_3OD held at 125 K. For masses between 4 and 60, only the 4, 18, 30, 34, and 36 amu signals exhibited increases in response to the electron beam, and these were very small. Because of background at 2 amu, we could not establish whether atomic D is ejected. Consistent with XPS (below) the integrated signals indicate that no more than 0.05 ML of C- and O- containing species are removed in 600 s irradiation.

Product TPD after Electron Irradiation. When CD_3OD was irradiated, TPD revealed contributions from D_2O and/or CD_4, D_2, and CD_2O. Since the contributions from D_2O and CD_4 could not be separated because of overlapping peaks, we used

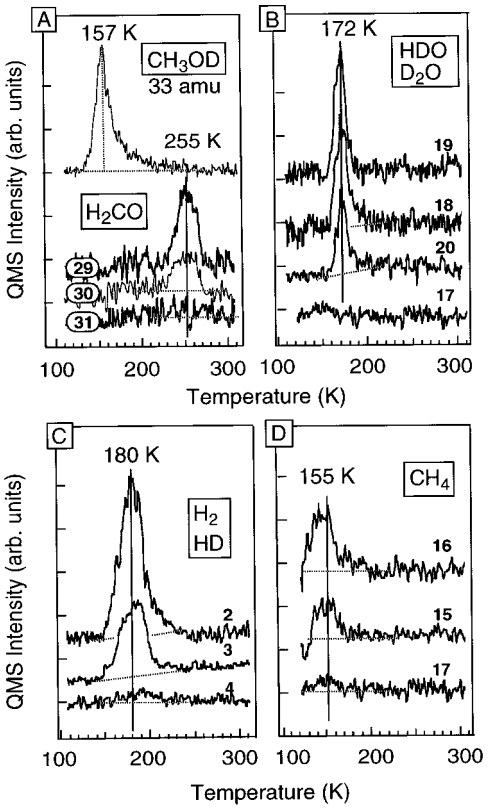

Figure 7. Four panels exhibit TPD spectra after irradiation of 1 ML of CH_3OD with $4.5 \times 10^{+16}$ e^- cm^{-2}. Panel A shows the residual parent (33 amu) and formaldehyde. Panel B shows the isotopically labeled water desorption, panel C the dihydrogen isotopes, and panel D the methane mass range. The text discusses the experimental difficulty with the peaks in panel D.

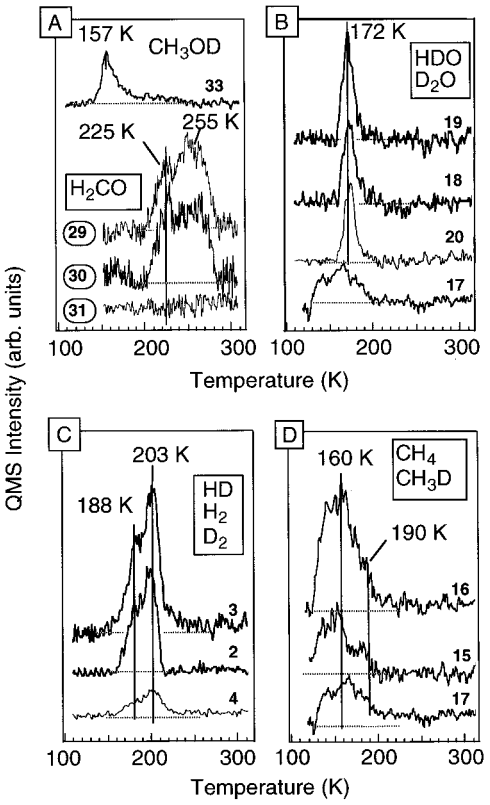

Figure 8. As in Figure 9, except with an electron fluence of $1 \times 10^{+17}$ e^- cm^{-2}.

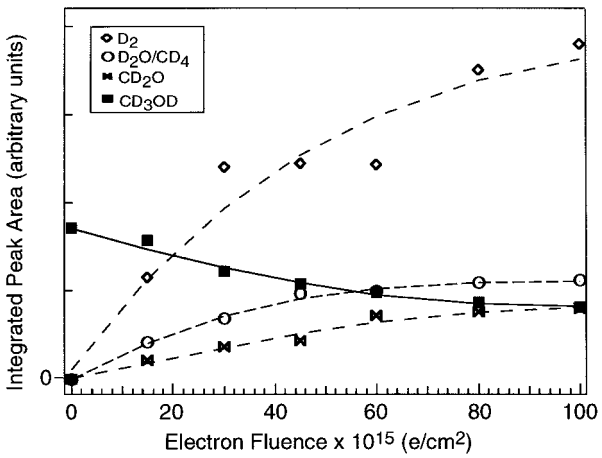

Figure 9. Plots of the evolution of hydrogen, water/methane, and formaldehyde and loss of methanol with increasing electron fluence. The lines (dotted and solid) are to guide the eye.

labeled methanol, CH_3OD. Monolayer TPD for CD_3OD and CH_3OD (no electron irradiation) had identical peak shapes and temperatures indicating, as expected, that hydrogen atom motions are not critical in the reaction coordinate leading to parent desorption.

Electron Irradiation of CH_3OD. Figure 7 shows the product TPD spectra taken after irradiation of monolayer CH_3OD with 4.5×10^{16} e^- cm^{-2} of 52 eV electrons. This fluence reduces the parent TPD signal (33 amu) to 0.65 of its initial value (panel A and Figure 5). Throughout the temperature interval of the 157 K desorption peak, the signal fragmentation pattern (not shown) matches that for CH_3OD.

The formaldehyde peaks contain no detectable deuterium; the 31 amu signal, $CDHO^+$, is negligible (panel A). Thus, even though D is present, intermediates leading to formaldehyde seldom, if ever, involve C−D bonds. Panel B plots the thermal desorption profiles (background subtracted) of 17, 18, 19, and 20 amu; since 17 is negligible, we attribute the 172 K peaks in 18, 19, and 20 amu to two isotopic forms of water, HDO and D_2O, and eliminate partially deuterated methane (CH_3D) desorption as a possible contributor.

Panel C profiles the isotopic dihydrogen desorptions, which are ordered $H_2 > HD \gg D_2$. The minimal D_2 desorption and the relatively small HD desorption confirm a strong preference for electron-induced C−H bond breaking.

Panel D, which shows traces for masses attributable to methane, is difficult to analyze. There is no literature evidence for a reaction between adsorbed H and CH_3 at such low temperatures; this route to methane formation typically does not contribute below 200 K.[7,55,56] Further, there is no analogous low-temperature CD_4 signal in the data taken using CD_3OD as the adsorbate. Keeping in mind that the ion pumped system routinely regurgitates small and somewhat variable amounts of CH_4, 16 amu, we assign the low-temperature peaks in panel D to background sources and discuss them no further.

When the fluence was increased to $1 \times 10^{+17}$ e^- cm^{-2}, similar TPD measurements, Figure 8, exhibit only a few notable differences: (1) there is a detectable 17 amu signal (panel B) which spans, but does not track, the water desorption; (2) the formaldehyde signal now has two peaks; (3) the dihydrogen has two peaks, with $HD > H_2 \gg D_2$; and (4) even after discounting the low-temperature 16 amu signal at 160 K, additional signal appears around 190 K that is ascribed to CH_4 desorption and, for 17 amu, to CH_3D desorption.

Figure 9 shows how the TPD peak areas varied with fluence when monolayer CD_3OD was irradiated. Taking the CD_3OD and CH_3OD data together, the qualitative picture described in Scheme 2 emerges for fluences up to $4.5 \times 10^{+16}$ e^- cm^{-2}. For

higher fluences, the dihydrogen and formaldehyde desorptions continue to grow as additional parent is consumed, while the sum of water plus methane tends to saturate. Significantly, the isotopic distribution of dihydrogen shifts to involve more D atoms. This may be the result of producing $D_{(a)}$ during electron irradiation or TPD and D-for-H exchange during TPD.

Fluence Dependence of Reaction Products. With the isotopic labeling results in mind, we turn to a more detailed discussion of the fluence dependence of the reaction. As the parent signal decays, the 20 amu signal rises monotonically, (Figure 9). As is clarified by the isotope labeling experiments, this region is dominated by D_2O desorption, with a small contribution from CD_4 on the high-temperature side (∼190 K). By way of comparison, CH_4 desorption after electron irradiation of biacetyl, $CH_3COCOCH_3$, peaks at 235 K.[7]

In the temperature interval where the 20 amu signal is strongest, 170−190 K, the D_2 signal rises, and its intensity increases monotonically with fluence (Figure 9). Based on the isotope labeling study, this D_2 is derived mainly from electron-induced C−D bond breaking, especially for low fluences. While recombinative D_2 desorption from Ag(111) occurs in this region,[57] a significant portion of the D_2 observed here involves one or more reaction-limited, thermally activated dehydrogenation processes that become active in this temperature interval. These include O−D cleavage.

After the water and dihydrogen signals have decayed, the formaldehyde (Figure 8) desorption begins around 225 K, maximizes at 255 K, and decays back to baseline at 270 K. A second H_2CO peak, centered at 225 K, appears when the fluence is doubled (Figure 8). This new peak overlaps with dihydrogen desorption, and the two may be related via O−D or C−H bond breaking. According to Figure 9, the total amount of desorbed D_2CO increases with electron fluence, but the 255 K peak saturates at 4.5×10^{16} e^- cm^{-2} and subsequent growth is slow and involves only the 225 K peak (Figures 7 and 8).

We propose that the high-temperature H_2CO arises from the decomposition of oligomerized formaldehyde, $-[H_2CO]_n-$, while the low-temperature peak is from reaction-limited decomposition of $H_2C_{(a)}O_{(a)}D$ fragments formed in localities where the coverage of fragments is high enough to impede the formation of additional oligomers.

Other Desorption Products. A detailed examination of other masses (2−60 amu) for a fluence of 4.5×10^{16} e^- cm^{-2} reveals no other contributions. The absence of acetaldehyde, acetone, and methyl ether, D_3COCD_3, is demonstrated by unpeaked signals at 46, 48, 50, and 52 amu.

Work Function Changes with Electrons. Figure 4 shows that exposure of 1 ML of CH_3OD to 4.5×10^{16} (open squares) and 1×10^{17} e^- cm^{-2} (diamonds) at 120 K raises $\Delta\Phi$ from −1.0 to −0.6 and −0.25 eV, respectively. Since, acccording to XPS (below), very little C or O is ejected during irradiation, the work function change indicates a shift of electron density toward the vacuum side of the interface due to strong substrate bond formation, particularly silver−oxygen bonds (Scheme 2B). For 1×10^{17} e^- cm^{-2}, $\Delta\Phi$ increases further. We take this to imply additional strong Ag−O bonds in $D_2C_{(a)}O_{(a)}D$ or $CD_3O_{(a)}$, the latter formed by O−D bond breaking.

Upon heating after irradiation, $\Delta\Phi$ also rises. The small drop between 200 and 220 K for the $4.5 \times 10^{+16}$ e^- cm^{-2} case correlates with the partial oxidation process that leads to the desorption of D_2 in TPD. Its absence after more extensive irradiation may reflect increased electron-induced O−D bond breaking as primary products accumulate. At 285 K, the work function of the two irradiated surfaces indicates the presence of some residual material, probably $O_{(a)}$, which makes $\Delta\Phi$ slightly positive, but by 450 K, $\Delta\Phi = 0.00$ eV as expected for clean Ag(111).

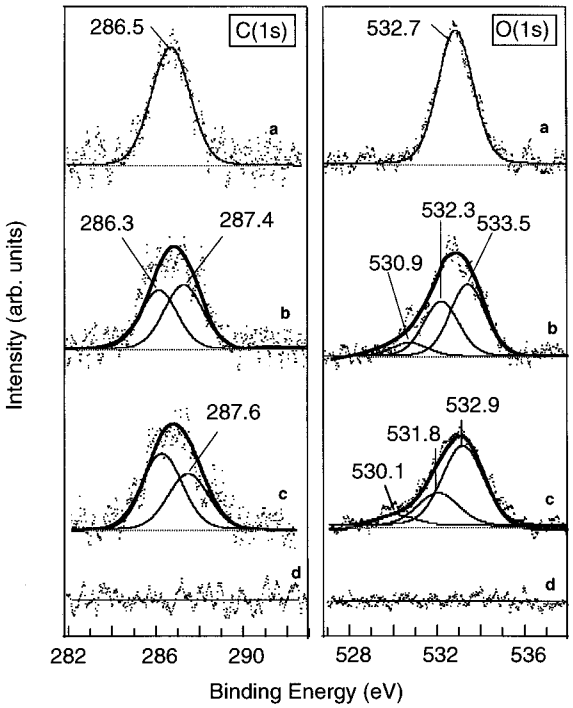

Figure 10. C(1s) and O(1s) XPS before (a) and after exposing 1 ML of CD_3OD to $4.5 \times 10^{+16}$ (b) and $1 \times 10^{+17}$ e^- cm^{-2} (c). After heating to 450 K, spectra (d) are obtained.

X-ray Photoelectron Spectroscopy. XPS confirms, through altered core level binding energy distributions, that electron irrradiation changes the chemical character of the carbon and oxygen making up the adsorbate layer. Figure 10 shows the C(1s) and O(1s) XPS for 1 ML of CH_3OD before (curves a) and after exposure to $4.5 \times 10^{+16}$ (curves b) and $1 \times 10^{+17}$ e^- cm^{-2} (curves c). Scans after heating the irradiated samples to 450 K are indistiguishable from clean surface spectra (curves d). The spectra taken before irradiation agree with those shown for monolayer coverage in curves b of Figure 3. After electron exposure, the C(1s) and O(1s) peak intensities drop, but only slightly, with a slightly higher loss for the larger fluence. C-(1s) drops from 1.0 to 0.96 to 0.94; O(1s) drops a bit further, but no more than 10% at the highest fluence. Increasing irradiation clearly shifts the O(1s) distribution toward lower BE which, as for $\Delta\Phi$, is consistent with stronger O−Ag coupling in the products. C(1s) broadens more on the high binding energy (BE) side. With increasing fluence, the C(1s) spectra are readily fit (G−L = 90%−10%) with two C(1s) peaks, both with fwhm of 2.0 eV, centered at 286.5 ± 0.2 and 287.6 ± 0.2 eV. The fits to the O(1s) spectra require three separate peaks to account for the width, and there is a drift toward lower BE with fluence—530.9, 532.3, and 533.5 eV for $4.5 \times 10^{+16}$ e^- cm^{-2}, and for $1.0 \times 10^{+17}$ e^- cm^{-2}, 530.1, 531.8, and 532.9 eV.

The spectra of Figure 10, while verifying electron-induced alteration of adsorbed CD_3OD, are clearly comprised of strongly overlapping features that cannot be resolved unambiguously.

XPS after Irradiation and Annealing. Figure 11 summarize XPS data taken after annealing electron-irradiated monolayers with $4.5 \times 10^{+16}$ e^- cm^{-2}. Based on analogous TPD, very few O−D bonds are broken, the dihydrogen and formaldehyde TPD spectra have only a single peak, and there is little, if any, evidence for methane. Upon annealing to 175 K (curves 11a), the C(1s) peak area drops to 0.40 ± 0.04 and O(1s) to 0.45 ± 0.04 of their initial values (Figure 10b). The C(1s) BE is

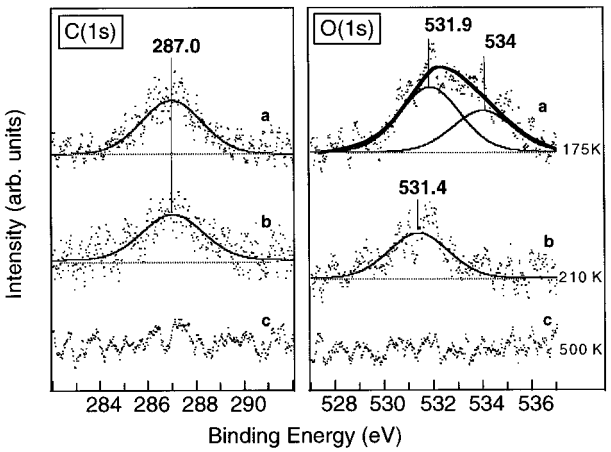

Figure 11. C(1s) and O(1s) XPS after exposing 1 ML of CD_3OD to $4.5 \times 10^{+16}$ (curve b of Figure 10) and then annealing to (a) 175, (b) 210, and (c) 500 K.

unchanged (287.0 eV), but the O(1s) shifts and broadens from 532.7 eV toward higher and lower BE and requires only two peaks (531.9 and 534 eV) for an acceptable fit. Heating to 210 K (curves b) reduces the C(1s) and O(1s) intensities to 0.31 ± 0.03 and 0.27 ± 0.03 of their initial values. The high BE portion of the O(1s) intensity is lost, leaving one peak at 531.4 eV. Heating to 500 K (curves c) reduces both signals below detection limits.

According to postirradiation TPD, 0.65 ± 0.05 of the initial coverage of CD_3OD desorbs after $4.5 \times 10^{+16}$ e^- cm^{-2} (Figure 9). This compares very favorably with XPS since most, but not all, the residual parent desorbs by 175 K (Figure 5). In TPD, all the residual parent, dihydrogen, and water desorb by 210 K (Figure 7), leaving only the formaldehyde precursor. This is consistent with the 1 C: 1 O stoichiometry and the single BE peaks in XPS. We conclude that a fluence of $4.5 \times 10^{+16}$ e^- cm^{-2} and subsequent annealing to 210 K leaves about 0.30 ML of the precursor as oligomeric $-(CD_2O)_n-$ (Scheme 2). TPD shows that heating to 500 K is sufficient to desorb all the formaldehyde and, according to XPS, leaves a clean surface. We conclude that, for this irradiation and annealing, the binding energies for the formaldehyde precursor lie at 287.0 for C(1s) and 531.4 eV for O(1s).

An XPS annealing set (not shown) after irradiation with $1.0 \times 10^{+17}$ e^- cm^{-2} is also consistent with the TPD results. Upon annealing to 185 K, desorbing parent and some D_2O, the O(1s) signals drop to 0.40 of its initial value, compared to 0.53 for C(1s). Upon annealing to 195 K, there is a differential reduction favoring carbon—C(1s) drops by 0.13 to 0.40 ± 0.04 and O(1s) by 0.08 to 0.32 ± 0.04. This is accompanied by slight broadening toward lower BE. Further annealing to 215 K leaves 0.30 C(1s) and 0.31 O(1s), and annealing to 450 K removes the remaining C and O.

Variation with Initial Coverage. In other experiments, we briefly examined the effect of decreasing (0.4 ML) and increasing (2 ML) the initial coverage (CH_3OD) while holding the electron fluence constant ($1 \times 10^{+17}$ e^- cm^{-2}). For 0.4 ML, the products and desorption temperatures (not shown) are nearly the same as those detected for the 1 ML case. The only notable difference was that D_2 was barely detectable in the dihydrogen isotopic distribution. Just as for 1 ML, lowering the fluence to $4.5 \times 10^{+16}$ e^- cm^{-2} reverses the order, $H_2 >$ HD, while D_2 remains below detection limits.

When irradiating 2 ML, the parent TPD signal decreased much more rapidly than for 1 ML. Increased initial loss is attributed to electron-stimulated desorption of parent from the upper methanol layers, a phenomenon observed for CH_3OH multilayers adsorbed on metal oxides.[58] Except for formaldehyde which was highest for 1 ML, TPD product intensities generally increased with initial coverage, but increases between 0.4 and 1 ML were larger than between 1 and 2 ML. These results suggest that parent and/or fragment ejection during irradiation becomes more important in the multilayer region. Unfortunately, XPS data are not available to test for loss of C and O. We cannot explain why the maximum CH_2O intensity appears for 1 ML, but it may be related to the limited formation of oligomers of formaldehyde.

The 2 ML CH_3OD TPD results also contain evidence for a new desorption product. After irradiation with 1×10^{17} e^- cm^{-2}, the 31 amu signal peaks at 175 K and is accompanied by companion traces for 29, 16, and 17 amu. Possible candidates for this new species, based on the appearance of 31 amu, are methyl formate and/or glycolaldehyde. Both of these molecules have a significant contribution from 29 and 31 amu (~50 and 100% of the parent ion intensity). The parent mass, 60 amu, was not monitored, so no unambiguous assignment is possible at this point, but we note that glycolaldehyde appears in TPD when methyl formate is irradiated with electrons.[47]

4. Discussion

4.1. Thermal Chemistry. Consistent with our monolayer XPS BE's, 286.5 and 532.7 eV, Jenniskens et al.[52] found C(1s) and O(1s) spectra characteristic of a single species with monolayer BE's of 286.4 and 532.8 eV. On Ag(111),[45] Pt(110),[29] Cu(110),[39] Ni(110),[9] and Pd(100),[59] the calculated absolute monolayer coverage lies between $5 \times 10^{+14}$ and $8.4 \times 10^{+14}$ cm^{-2}, in good agreement with our calculated value of $8 \times 10^{+14}$ cm^{-2} from calibrated XPS results.

Consistent with the literature,[52] we find that methanol adsorbs and desorbs without decomposition on Ag(111), that the monolayer desorption activation energy is 0.40 ± 0.02 eV = 38.6 ± 1.9 kJ mol^{-1}, and that monolayer and multilayer peaks are readily resolved. A third desorption associated with the second and third layers and attributed to amorphous CD_3OD, presumably thermodynamically metastable, was also distinguished.[52] We did not resolve this feature, perhaps either because the ramp rate, 1.5 K s^{-1}, was slow enough to allow the metastable phase to relax or because our adsorption temperature was higher, 120 vs 110 K.

There is one other interesting difference with earlier work[52] in the behavior of the sticking coefficient: we find an increase in passing from monolayer to multilayer, whereas earlier investigators found a constant value throughout, perhaps because of 10 K lower adsorption temperature. To account for the increased sticking coefficient in multilayers, we suppose that once accommodated to Ag(111), submonolayer CD_3OD is weakly oriented with its oxygen lone pair toward the substrate (Scheme 1). If CD_3OD approaches with the methyl group toward the bare Ag, the forces leading to orientation with O toward the surface and to the energy redistribution needed for accommodation are not very effective, and a sizable fraction of the incident CD_3OD returns to the gas phase. If, on the other hand, arriving CD_3OD encounters previously adsorbed CD_3OD rather than Ag(111), there are different energy exchange and accommodation opportunities. The repulsive potentials may rise much less steeply, allowing more time for energy transfer, the orientation requirements may be less restrictive, and hydrogen-bonding forces may promote energy exchange. The net result is a higher sticking probability.

The model suggested above for the orientation of adsorbed monolayer CD_3OD (Scheme 1), is consistent with the work

function change measurements and with all the literature. The dipole moment of isolated CD_3OD is 1.70 D, and since the binding is very weak, we assume very little change upon adsorption. The measured work function change can then be used to estimate the projection of the dipole moment along the surface normal (per adsorbed CD_3OD). This calculation makes use of the molecular polarizability of methanol, 3.25 Å,[3] and the Topping relation:[60]

$$\Delta\Phi = \frac{n_s{}^0\mu_s}{\epsilon^0(1+9\alpha n_s)^{3/2}}$$

where ${}^0\mu_s$ is the extrapolated dipole moment at zero coverage. Solving gives ${}^0\mu_s = 0.57$ D, a factor of 3 lower than the dipole moment of isolated CD_3OD; this indicates that the C−O axes of adsorbed monolayer CD_3OD molecules tilt with respect to the surface normal, as in Scheme 1.

Electron-Induced Chemistry. It is clear from the combination of TPD, XPS, and ΔΦ measurements that significant bond dissociation occurs when CD_3OD and CH_3OD are irradiated with ca. 50 eV electrons. While for multilayers there is circumstantial evidence for parent removal, for initial coverages ≤1 ML, there is little electron-induced removal of C− or O-containing species.

The calculated total cross section for loss of CD_3OD is an order of magnitude lower than for loss of ethylene[55] or biacetyl.[57] This is ascribed to stronger electronic coupling to the substrate of the neutral ground and, particularly, ionic excited state(s) of CD_3OD compared to the other adsorbates. The highest lying occupied orbital in CD_3OD is strongly localized on the oxygen, i.e., lone pair, which is also heavily involved in the linkage to Ag. For 1 ML or less, ionization from this orbital will prepare a cation preoriented for substrate-mediated quenching.

This line of reasoning is consistent with there being very little ejection during irradiation of CD_3OD. In contrast, irradiation of biacetyl ($CH_3COCOCH_3$) leads to strong ejection of CO and CH_3, probably because its larger size moves it further from the surface, lengthening the cationic lifetime and making the dissociation cross section higher and ejection more competitive. The CD_3OD orientation, CD_3 toward the vacuum, would favor ejection provided the C−O bond in CD_3OD^+ accumulated the requisite energy before quenching, ca. 340 kJ mol^{-1} = 3.5 eV. Apparently this does not occur readily. Similar considerations apply to C−D bond dissociation and ejection. Unfortunately, as noted in section 3, we could not determine whether atomic D is ejected. Even if the requisite energy for ejection does not accumulate before quenching, C−D and C−O dissociation can occur afterward if enough vibrational energy accumulates. Since the substrate can lower the activation barrier to dissociation on the ground-state potential energy surface through Ag−CD_3, Ag−OD, and Ag−D coupling, with sufficient vibrational energy to surmount the activation barrier, these couplings would lead to dissociation and bound fragments, as observed.

Regarding the retained fragments, the BE's lie between 286.6 and 289.1 eV for C(1s) and between 530.1 and 534 for O(1s). These ranges encompass reported BE's for the species we propose in Scheme 2 (and many others as well). For oxygen-bearing organic fragments such as those being dealt with here, C(1s) BE's typically range from 284.5 eV for methylene groups upward to 288 eV for carbonyls. The O(1s) BE's range from 530 eV for adsorbed atomic oxygen to 534 eV for ethers.[51] This range omits carbides, graphitic carbon, carboxyl, oxide, and peroxide moieties, none of which are evident in our work.

Except for long irradiation times, where approximately half an initial monolayer of CD_3OD remains (TPD), the full C(1s) intensity distribution peaks within 0.2 eV of 286.9 eV, and forcing resolution into multiple peaks based on fixed fwhm is justified only because there are changes in TPD and ΔΦ; i.e., the C(1s) XPS spectra cannot be used unambiguously to identify and distinguish surface products. There is clearer evidence for multiple species in the O(1s) spectra where, after irradiation, an asymmetry consistent with increased Ag−O bonding emerges on the low BE side (Figure 10). The overall O(1s) peaks lie within 0.2 eV of 532.7. As for C(1s), multiple peaks appear in part because we have used fits with fixed fwhm values.

The isotope labeling experiments clearly reveal a strong bias against O−D bond breaking, consistent with electron-induced gas-phase fragmentation. C−H bond dissociation implies that a fragment with the structure $H_xC_{(a)}-O_{(a)}D$ is formed. We assign BE's in the regions 287.4 and 533.5 eV to $H_2C_{(a)}-O_{(a)}D$. The O−Ag bond may be very weak compared to C−Ag.

The postirradiation TPD products are generally similar to those for methanol on oxygen-precovered Cu and Ag surfaces; however, with oxygen precoverage, adsorbed formate, $HCOO_{(a)}$, and additional desorption products—CO, CO_2, and methyl formate[3,43,61]—were found. As expected, Ag(111) does not behave like more active transition-metal surfaces (e.g., Ni, Pt, and Pd), which thermally decompose methanol and its fragments, leading to TPD of CO and H_2.[15,18,29,32]

After irradiation, the C(1s) and O(1s) BEs at ca. 287.4 and 531.5 eV are assigned to paraformaldehyde, $-(H_2CO)_n-$, known to result from either thermal [62−65] or UV excitation[66] of adsorbed formaldehyde. Paraformaldehyde decomposition to yield H_2CO has been observed at 235 K on Ag(110)[63] and 248 K on Pt(111).[64] This agrees well with the H_2CO TPD here.

While electron activated O−D bond breaking is not included in Scheme 2, we have suggested that it contributes in the later stages of irradiation and annealing. The resulting methoxy fragments are well-established in the thermal decomposition of CD_3OD in the presence of $O_{(a)}$ on Ag substrates.[3] It is, thus, likely that this channel is enhanced when CD_3OD^+ forms in the presence of previously formed products. In particular, species involving strong O−Ag bonds could mimic the local Lewis acid−base environment that is critical for thermal methoxide formation on oxygen-covered Ag. This kind of process could lead to fragment linkages, e.g., $CD_3O + CH_2O$, to form hemiacetal alcoholate,[45] and to higher molecular weight TPD products of the kind thought to contribute after extensive irradiation of 2 ML.

Final Note Regarding Photochemistry. A comment on the photochemistry of CH_3OH adsorbed on Ag(111) is appropriate. Unpublished work in our laboratory found, using an unfiltered Hg arc (≥240 nm), no evidence for photon-stimulated desorption or dissociation.[67] The absence of photochemistry has been confirmed at 355 nm in other work.[68] Even when photons are not absorbed by methanol, irradiation leads to hot carrier production in the substrate and, for the Hg arc, photoelectron ejection. Consistent with Figure 6, these low-energy electrons (≤1.5 eV) do not activate bond breaking in adsorbed CH_3OH.

5. Summary

The results of this investigation are summarized as follows:

1. On Ag(111) at 120 K, methanol (CH_3OD and CD_3OD) adsorbs and desorbs without dissociation and reaches monolayer coverage at $8 \times 10^{+14}$ cm^{-2}.

2. Above 12.5 eV, electron irradiation leads to dissociation without the ejection of significant carbon- or oxygen-containing species.

3. At 50 eV the cross section is $(7.8 \pm 0.4) \times 10^{-18}$ cm^{+2}, an order of magnitude lower than for biacetyl and ethylene.

This difference is explained in terms of factors that control the quenching rate—orientation and average distance from the surface.

5. Products (and peak temperatures) observed in TPD include water (172 K), methane (190 K), dihydrogen (188 and 203 K), and formaldehyde (225 and 255 K).

6. From isotope labeling using CH_3OD, the following conclusions emerge: (i) electron-induced O−D cleavage makes, at most, a small contribution, especially in the early stages of irradiation; (ii) paths by which formaldehyde forms involve negligible deuterium; and (iii) thermally activated processes among adsorbed fragments lead to water and dihydrogen that incorporate D.

7. The two formaldehyde TPD features are attributed to reaction-limited formation and desorption (225 K) and decomposition of paraformaldehyde (255 K).

Acknowledgment. This work was supported by in part by the U.S. Department of Energy, Office of Basic Energy Sciences, and by the Robert A. Welch Foundation.

References and Notes

(1) *Formaldehyde*; Walker, J. F., Ed.; Reinhold: New York, 1964; pp 1−36.
(2) An early reference is Sexton, B. A. *Surf. Sci.* **1979**, *88*, 299.
(3) Wachs, I. E.; Madix, R. J. *J. Catal.* **1980**, *53*, 190.
(4) The subscript "(a)" is used to designate atoms bound to Ag.
(5) Zhou, X.-L.; Zhu, X.-Y.; White, J. M. *Surf. Sci. Rep.* **1991**, *13*, 73.
(6) *Laser Spectroscopy and Photochemistry on Metal Surfaces*; Dai, H.-L.; Ho, W., Eds.; World Scientific: Singapore, 1995; Part II and references therein.
(7) Pylant, E. D.; Hubbard, M. J.; White, J. M. *J. Phys. Chem.* **1996**, *100*, 15890.
(8) Richter, L. J.; Ho, W. *J. Chem. Phys.* **1985**, *83*, 2569.
(9) Bare, S. R.; Stroscio, J. A.; Ho, W. *Surf. Sci.* **1985**, *150*, 399.
(10) Demuth, J. E.; Ibach, H. *Chem. Phys. Lett.* **1979**, *60*, 395.
(11) Rubloff, G. W.; Demuth, J. E. *J. Vac. Sci. Technol.* **1977**, *14*, 419.
(12) Johnson, S.; Madix, R. J. *Surf. Sci.* **1981**, *103*, 361.
(13) Baudais, F. L.; Borschke, A. J.; Fedyk, J. D.; Dignam, M. *J. Surf. Sci.* **1980**, *100*, 210.
(14) Yates, J. T., Jr.; Goodman, D. W.; Madey, T. E. In *Proc. 7th Intern. Vacuum Congr. and Intern, Conf. on Solid Surfaces, Vienna, 1977*; p 1133.
(15) Christmann, K.; Rustig, J. *8th International Congress on Catalysis, Proceedings*, 1984; Vol. IV, pp 13−25.
(16) Kojima, I.; Sugihara, H.; Miyazaki, E.; Yasumori, I. *J. Chem. Soc., Faraday Trans. 1* **1981**, *77*, 1315.
(17) Christmann, K.; Demuth, J. E. *J. Chem. Phys.* **1982**, *76*, 6318.
(18) Davis, J. L.; Barteau, M. A. *Surf. Sci.* **1988**, *197*, 123.
(19) Gates, J. A.; Kesmodel, L. L. *J. Catal.* **1983**, *83*, 437.
(20) Benziger, J. B.; Madix, R. J. *J. Catal.* **1980**, *65*, 36.
(21) Lu, J.-P.; Albert, M.; Bernasek, S. L. *Surf. Sci.* **1989**, *218*, 1.
(22) Lu, J.-P.; Albert, M. R.; Bernasek, S. L. *Surf. Sci.* **1991**, *258*, 269.
(23) Albert, M. R.; Lu, J.-P.; Bernasek, S. L.; Dwyer, D. J. *Surf. Sci.* **1989**, *221*, 197.
(24) McBreen, P. H.; Erley, W.; Ibach, H. *Surf. Sci.* **1983**, *133*, L469.
(25) Miles, S. L.; bernasek, S. L.; Gland, J. L. *J. Phys. Chem.* **1983**, *87*, 1626.
(26) Hrbek, J.; De Paola, R.; Hoffmann, F. M. *Surf. Sci.* **1986**, *166*, 361.
(27) Deckert, A. A.; Brand, J. L.; Mak, C. H.; Koehler, B. G.; George, S. M. *J. Chem. Phys.* **1987**, *87*, 1936.
(28) Berko, A.; Tarnoczi, T. I.; Solymosi, F. *Surf. Sci.* **1987**, *189*, 238.
(29) Attard, G. A.; Chibane, K.; Ebert, H. D.; Parsons, R. *Surf. Sci.* **1989**, *224*, 311.
(30) Kizhakevariam, N.; Stuve, E. M. *Surf. Sci.* **1993**, *286*, 246.
(31) Sexton, B. A. *Surf. Sci.* **1981**, *102*, 271.
(32) Peremans, A.; Maseri, F.; Darville, J.; Gilles, J.-M. *Surf. Sci.* **1990**, *227*, 73.
(33) Egelhoff, W. F.; Linnett, J. W.; Perry, D. L. *Faraday Discuss. Chem. Soc.* **1975**, *60*, 122.
(34) Chen, J. G.; Basu, P.; Ng, L.; Yates, J. T., Jr. *Surf. Sci.* **1988**, *194*, 397.
(35) Sheu, B.-R.; Strongin, D. R. *Langmuir* **1994**, *10*, 1801.
(36) Rogers, J. W.; Jr., Hance, R. L.; White, J. M. *Surf. Sci.* **1980**, *100*, 388.
(37) Basu, P.; Chen, J. G.; Ng, L.; Colaianni, M. L.; Yates, J. T., Jr. *J. Chem. Phys.* **1988**, *89*, 2406.
(38) Sexton, B. A. *Surf. Sci.* **1979**, *88*, 299. Sextion, B. A.; Hughes, A. E. *Surf. Sci.* **1984**, *140*, 227.
(39) Bowker, M.; Madix, R. J. *Surf. Sci.* **1980**, *95*, 190.
(40) Peremans, A.; Maseri, F.; Darville, J.; Gilles, J.-M. *J. Vac. Sci. Technol. A* **1990**, *8*, 3224.
(41) Russell, J. N.; Jr., Gates, S. M.; Yates, J. T., Jr. *Surf. Sci.* **1985**, *163*, 516.
(42) Zhang, R.; Gellman, A. J. *J. Phys. Chem.* **1991**, *95*, 7433.
(43) Wachs, I. E.; Madix, R. J. *Surf. Sci.* **1978**, *76*, 531.
(44) Dai, Q.; Gellman, A. J. *Surf. Sci.* **1991**, *257*, 103.
(45) Felter, T. E.; Weinberg, W. H.; Lastushkina, G. Y.; Zhdan, P. A.; Boreskov, G. K. *Appl. Surf. Sci.* **1983**, *16*, 351.
(46) Bao, X.; Deng, J.; Zhai, R.; Wang, D.; Guo, X. *Catal. Lett.* **1990**, *4*, 25.
(47) Schwaner, A. L.; Fieberg, J. L.; White, J. M. *J. Phys. Chem.*, submitted.
(48) Converse-Sparks, S.; Szabo, A.; Szulczewski, G. J.; Junker, K.; White, J. M. To be published.
(49) McLafferty, F. W.; Stauffer, D. B. *The Wiley/NBS Registry of Mass Spectral Data;* Wiley: New York, 1989; Vol. 1.
(50) Gerenser, L. J.; Baetzold, R. C. *Surf. Sci.* **1980**, *89*, 259.
(51) Muilenberg, G. E. In *The Handbook of X-ray Photoelectron Spectroscopy;* Perkin-Elmer: Eden Prairie, Mn, 1979.
(52) Jenniskens, H. G.; Dorlandt, P. W. F.; Kadodwala, M. F.; Kleyn, A. W. *Surf. Sci.* **1996**, *357*, 624.
(53) Tanaka, K.; Matsuzaki, S.; Toyoshima, I. *J. Phys. Chem.* **1993**, *97*, 5673.
(54) *CRC Handbook of Chemistry and Physics*; 52nd ed; Chemical Rubber Co.: Clevelend, 1971; p E64.
(55) Zhou, X.-L.; Schwaner, A. L.; White, J. M. *J. Am. Chem. Soc.* **1993**, *115*, 4309.
(56) Zhou, X.-L.; White, J. M. *J. Phys. Chem.* **1992**, *97*, 7703.
(57) Zhou, X.-L.; White, J. M.; Koel, B. E. *Surf. Sci.* **1989**, *218*, 201.
(58) Au, C. T.; Hirsch, W.; Hirschwald, W. *Surf. Sci.* **1989**, *221*, 113.
(59) Christmann, K.; Demuth, J. E. *J. Chem. Phys.* 1**982**, *76*, 6308.
(60) *Low Energy Electrons and Surface Chemistry*; Ertl, G., Kuppers, J., Eds.; Verlag Chemie: Weinheim, 1974; p 125.
(61) Barteau, M. A.; Madix, R. J. *Surf. Sci.* **1982**, *120*, 262.
(62) Sexton, B. A.; Hughes, A. E.; Avery, N. R. *Surf. Sci.* **1985**, *155*, 366.
(63) Stuve, E. M.; Madix, R. J.; Sexton, B. A. *Surf. Sci.* **1982**, *119*, 279.
(64) Henderson, M. A.; Mitchell, G. E.; White, J. M. *Surf. Sci.* **1987**, *188*, 206.
(65) Sen, P.; Rao, C. N. R. *Surf. Sci.* **1986**, *172*, 269.
(66) Fleck, L. E.; Feehery, W. F.; Plummer, E. W.; Ying, Z. C.; Dai, H. L. *J. Phys. Chem.* **1991**, *95*, 8428.
(67) Pressley, L. A.; Coon, S. R.; White, J. M. unpublished. See also: Zhou, X.-L.; Zhu, X.-Y.; White, J. M. *Surf. Sci. Rep.* **1991**, *13*, 73 especially Table 1, p 146.
(68) Jenniskens, H. private communication. See also ref 52.